

NUMERICAL PREDICTIONS ON THE DYNAMIC RESPONSE OF A SUSPENSION BRIDGE WITH A TRAPEZOIDAL CROSS-SECTION

Fuh-Min Fang*, Yi-Chao Li, Chu-Chang Chen, Tsung-Chi Liang, and Jwo-Hua Chen

ABSTRACT

A numerical method is developed to predict the dynamic behavior of a suspension bridge under wind action in a two dimensional sense. In particular, the behavior of a vibrating deck with a trapezoidal cross-section is examined. The simulations contain two parts of computations, which are performed alternatively during the calculation process. The solutions of the instantaneous flow field and the deck motions are considered the basis to analyze the problem of deck instability.

Wind tunnel measurements are conducted in parallel to measure the response of a sectional bridge model. The vertical and torsional deflections of the model are measured under various wind speeds with several selected attack angles. The results are used to confirm the accuracy of the numerical predictions.

Results show that the numerical predictions of the structural response agree well with those from the experiments, indicating that the proposed method is capable of predicting the deck motion with good accuracy. Based on the time-series numerical results, finally, the interactive behavior of the vibrating trapezoidal deck is examined extensively.

Key Words: suspension bridge, numerical computation, wind tunnel test, section model, flutter derivatives.

I. INTRODUCTION

The instability of a suspension bridge under wind action is an important subject in wind engineering. In order to investigate the dynamic motion of the bridge deck as well as the corresponding wind effects, the method of model experiments is commonly used. Economically, however, the application of appropriate numerical methods can be another option. In addition, the numerical results can provide more extensive information for the analysis of such flow-structure interactive problems.

A number of researchers have investigated experimentally the mechanisms of wind-induced

vibration of suspension bridges. Typically, Scanlan and Tomko (1971) proposed a semi-experimental and semi-analytical approach regarding flutter derivatives, and this approach is presently widely used. Sarkar *et al.* (1992) suggested a system identification procedure to estimate all the flutter derivatives simultaneously. In their study, numerical simulations and reduction of the experimentally obtained direct derivatives are presented. Iwamoto and Fujino (1995) proposed a method of simultaneous identification of all eight flutter derivatives of bridge decks from free vibration data consisting of two modes. It is shown by experiments that an increase of mass and inertial moment of section model leads to better accuracy in identifying the flutter derivatives at high wind speeds. Based on the experimental results from a coupled vertical-torsional free vibration of a spring-suspended section model, Gu *et al.* (2000) employed the least-square theory and proposed an identification method to obtain flutter derivatives. Moreover, Noda *et al.* (2003) evaluated the flutter derivatives

*Corresponding author. (Tel: 886-4-22872221; Fax: 886-4-22862857)

F. M. Fang, Y. C. Li, C. C. Chen, and T. C. Liang are with the Department of Civil Engineering, National Chung-Hsing University, Taichung, Taiwan 402, R.O.C.

J. H. Chen is with the Department of Space Design, Chien-Kuo Institute of Technology, Chang-Hua, Taiwan 500, R.O.C.

Table 1 Related properties of present section model

Mass (M) (kg/m)	Moment of inertia (I) (kg-m ² /m)	Fundamental frequency (Hz)		Damping ratio (%)		β	U (m/s)
		Vertical	Torsional	Vertical	Torsional		
		(f_V)	(f_T)	(ξ_V)	(ξ_T)		
0.472	6.31×10^{-4}	14.8	28.4	0.80	0.70	$0^\circ, \pm 5^\circ, \pm 10^\circ$	2-18

of thin rectangular cylinders and found that the effect of oscillation amplitudes could be significant.

Besides wind tunnel tests, the application of computational fluid dynamics (CFD) is another way to assess the aerodynamic performance and aeroelastic stability of long span bridges. Kuroda (1997) presented a numerical simulation of high-Reynolds-number flows past a fixed section model with a shallow hexagonal cross-section. The overall characteristics of measured static force coefficients were well captured by the computations. Lee *et al.* (1997) investigated numerically the wind loading characteristics for turbulent flows over a two-dimensional bridge deck cross-section. The two-dimensional flow results were further used to perform three-dimensional dynamic structural analyses on a non-interactive basis. Fang *et al.* (2001) brought up a numerical method to simulate the surrounding flow and to predict the corresponding dynamic responses of a bridge deck with a rectangular cross-section. By employing a partially interactive procedure, the dynamic responses of the deck agreed well with the measurement results when the torsional responses were relatively insignificant.

In the study, a numerical model is proposed to simulate the dynamic response of a suspended bridge in a two-dimensional sense. Particularly, a bridge deck with a trapezoidal cross-section is assessed. In the numerical computations, two sets of equations, one for the simulation of the unsteady surrounding turbulent flow and the other for the calculation of the vibrating motions of the bridge deck, are solved alternatively to reflect the interaction effect between the structure and the flow by a completely interactive procedure. The resulting time-series responses of the structure as well as the wind loads are analyzed to examine the dynamic behaviors of the two. To verify the accuracy of the numerical results, on the other hand, wind tunnel experiments are conducted on a sectional deck model and the results of the vertical and torsional motions of the deck are used to confirm the numerical predictions.

Figure 1 depicts the schematic of the problem. The width of the upper surface of the trapezoid (B) is five times of the deck thickness (D). The mass distribution of the bridge cross-section is assumed

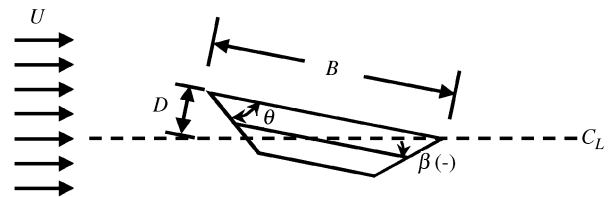


Fig. 1 Sketch of problem

uniform. Therefore, the effect due to eccentricity is not of concern. The inclined angle (θ) associated with the side surfaces of the trapezoidal deck cross-section is selected typically as 45° . With five attack angles (β ; $0^\circ, \pm 5^\circ$ and $\pm 10^\circ$), the approaching flow is considered smooth and the speed (U) varies from 2 to about 21.6 m/s (2 to 18 m/s for model experiments). Other related properties of the bridge deck are described in Table 1.

II. NUMERICAL METHOD

The simulations contain two parts of computations and are performed according to an interactive procedure. To predict the unsteady turbulent flow around the deck, a weakly-compressible-flow method (Song and Yuan, 1988) together with a dynamic subgrid-scale turbulence model (Germano *et al.*, 1991) is applied. After an instantaneous flow field is simulated, the resulting pressure distribution on the deck surfaces is integrated to obtain the wind load, which is taken as an input to further compute the corresponding structure responses. The resulting deflections and the vibrating speeds of the deck are then fed back to the boundary specifications of the deck surfaces for the flow calculations in the following time step. The alternative solutions of the instantaneous flow field and the deck motions in time series are considered to be the results of the interactive dynamic behaviors of the two.

1. Flow Calculations

In the weakly-compressible-flow method (Song and Yuan, 1988), the continuity and momentum equations are

$$\frac{\partial p}{\partial t} + k \nabla \cdot \mathbf{V} = 0 \quad (1)$$

$$\frac{\partial \mathbf{V}}{\partial t} + \mathbf{V} \cdot \nabla \mathbf{V} = - \nabla \frac{p}{\rho} + \nabla \cdot [(v + v_t) \nabla \mathbf{V}] \quad (2)$$

where p , \mathbf{V} and t denote respectively pressure, velocity and time; k is the bulk modulus of elasticity of air. v and v_t are respectively the laminar and turbulent viscosities, and the latter is determined based on a dynamic subgrid-scale turbulence model (Germano *et al.*, 1991). These two equations are further transformed into a coordinate system which goes with the motions of the bridge deck. Accordingly, as the coordinate systems are related by

$$\begin{aligned} X &= x \cos \alpha + y \sin \alpha \\ Y &= y \cos \alpha - x \sin \alpha - \int \dot{y}_v dt \end{aligned} \quad (3)$$

where (X, Y) and (x, y) are the spatial coordinates associated respectively with the new (moving) and the original (fixed) coordinate systems; y_v and α denote the vertical and torsional deflections of the deck; \dot{y}_v , $\dot{\alpha}$, are respectively the corresponding speeds in the vertical (cross-wind) and torsional directions, Eqs. (1) and (2) become

$$\begin{aligned} \frac{\partial p}{\partial t} + k [(\frac{\partial u}{\partial X} + \frac{\partial v}{\partial Y}) \cos \alpha + (\frac{\partial u}{\partial Y} - \frac{\partial v}{\partial X}) \sin \alpha] \\ + \frac{\partial p}{\partial X} (-\dot{\alpha} x \sin \alpha - \dot{\alpha} y \cos \alpha) \\ + \frac{\partial p}{\partial Y} (-\dot{\alpha} y \sin \alpha + \dot{\alpha} x \cos \alpha - \dot{y}_v) = 0 \end{aligned} \quad (4)$$

X-direction:

$$\begin{aligned} \frac{\partial u}{\partial t} + (u \frac{\partial u}{\partial X} + v \frac{\partial u}{\partial Y}) \cos \alpha + (u \frac{\partial u}{\partial Y} - v \frac{\partial u}{\partial X}) \sin \alpha \\ + [\frac{\partial u}{\partial X} (-\dot{\alpha} x \sin \alpha - \dot{\alpha} y \cos \alpha) \\ + \frac{\partial u}{\partial Y} (-\dot{\alpha} y \sin \alpha + \dot{\alpha} x \cos \alpha - \dot{y}_v)] \\ = - [\frac{\partial p}{\partial X} \cos \alpha + \frac{\partial p}{\partial Y} \sin \alpha] + (v + v_t) (\frac{\partial^2 u}{\partial X^2} + \frac{\partial^2 u}{\partial Y^2}) \end{aligned} \quad (5a)$$

Y-direction:

$$\begin{aligned} \frac{\partial v}{\partial t} + (u \frac{\partial v}{\partial X} + v \frac{\partial v}{\partial Y}) \cos \alpha + (u \frac{\partial v}{\partial Y} - v \frac{\partial v}{\partial X}) \sin \alpha \\ + [\frac{\partial v}{\partial X} (-\dot{\alpha} x \sin \alpha - \dot{\alpha} y \cos \alpha) \\ + \frac{\partial v}{\partial Y} (-\dot{\alpha} y \sin \alpha + \dot{\alpha} x \cos \alpha - \dot{y}_v)] \\ = - [\frac{\partial p}{\partial X} (-\sin \alpha) + \frac{\partial p}{\partial Y} \cos \alpha] + (v + v_t) (\frac{\partial^2 v}{\partial X^2} + \frac{\partial^2 v}{\partial Y^2}) \end{aligned} \quad (5b)$$

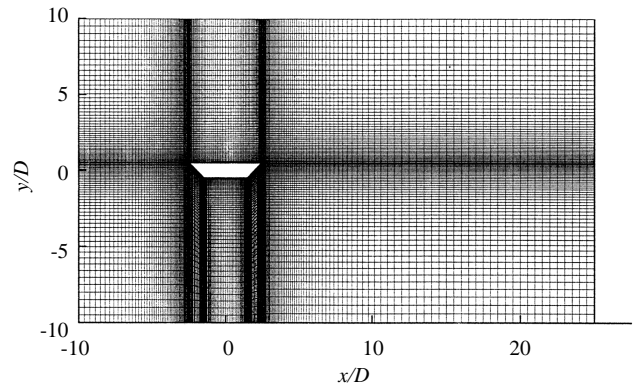


Fig. 2 Typical mesh system and domain of flow computations ($\beta=0^\circ$)

Based on Eqs. (4) and (5), the computation of the flow proceeds according to a finite-volume approach with an explicit finite-difference scheme. To ensure numerical stability, the time increment in the unsteady calculations is limited by the Courant-Friedrich-Lewy criterion (Courant *et al.*, 1967).

In the flow calculations, appropriate values of pressures and velocities are specified at exterior (phantom) grids outside the boundaries of the computational domain to reflect the physical nature of the boundaries. For the velocity specifications, since the computation is based on a non-stationary coordinate system, the boundary specifications at the deck surfaces have to account for the effect due to the instantaneous motion of the bridge deck. At the upstream inlet boundary, a smooth and uniform velocity profile together with an additional velocity caused by the coordinate transformations is imposed. At the other penetrable boundaries (side and exit boundaries of the flow domain), zero-gradient boundary specifications with a similar treatment due to the coordinate transformations are adopted. For the pressure specifications, on the other hand, the average pressure at the downstream section of the flow domain is chosen as the reference pressure. At the other penetrable and solid boundaries, the values at the phantom cells are given according to a zero-gradient assumption in the direction normal to the boundaries.

In all cases, the domain of flow calculations is in a rectangular shape ($38D \times 16D$ with a grid size of 242×88 ; see a typical mesh system in Fig. 2). The distances between the deck surfaces and the inlet as well as the exit are respectively $8D$ and $24D$, and a space of at least $7D$ is set between the deck and the side boundaries of the flow domain. By using these selections, preliminary numerical tests have shown that the relative error of the computational results is less than 2% (see Results).

2. Calculation of Bridge Responses

In the computations of the deck motions, the dynamic equations in the vertical (cross-wind) and torsional directions are respectively

$$\ddot{y}_v + 2\xi_v\omega_v\dot{y}_v + \omega_v^2y_v = \frac{F_L}{M} \quad (6)$$

$$\ddot{\alpha} + 2\xi_T\omega_T\dot{\alpha} + \omega_T^2\alpha = \frac{F_M}{I} \quad (7)$$

where \ddot{y}_v and $\ddot{\alpha}$ are the accelerations; M and I denote the mass and moment of inertia of the deck cross-section; F_L and F_M , obtained from the results of flow calculations, are respectively the wind loads in the cross-wind and torsional directions; ξ 's and ω 's denote the damping ratios and circular frequencies of the deck.

3. Flutter Derivatives

In the calculations of the deck responses, the forces induced by the deck motion are also examined in detail (see Discussion). For a 2-degree-of-freedom bridge deck, the lift and moment loads exerted on an oscillating bridge section induced by the vertical and torsional motions are given by the following equations (Scanlan and Tomko, 1971)

$$(F_L)_I = \rho U^2 B \left[KH_1^* \frac{\dot{y}_v}{U} + KH_2^* \frac{B\dot{\alpha}}{U} + K^2 H_3^* \alpha + K^2 H_4^* \frac{y_v}{B} \right] \quad (8)$$

$$(F_M)_I = \rho U^2 B^2 \left[KA_1^* \frac{\dot{y}_v}{U} + KA_2^* \frac{B\dot{\alpha}}{U} + K^2 A_3^* \alpha + K^2 A_4^* \frac{y_v}{B} \right] \quad (9)$$

where $K=2\pi f_v B/U$; B is the deck width; H_j^* and A_j^* ($j=1$ to 4) are the flutter derivatives.

Based on the time-series results of the numerical calculations, the flutter derivatives are obtained by the logarithmic-decrement method (Scanlan and Tomko, 1971) in this study. In addition, the initial vertical and torsional amplitudes of the bridge deck are selected respectively as $0.25D$ and 1.3° , which are considered reasonably small to avoid the amplitude effects (Noda *et al.*, 2003).

III. EXPERIMENTAL PROGRAM

A sectional deck model is installed on a suspended rack mechanism (see Fig. 3) in the test section ($80\text{ cm} \times 80\text{ cm}$) of a wind tunnel. The turbulence level (intensity) of the approaching flows in the tests is less than 0.5%. The thickness (D) and width (B) of the upper surface of the deck model are

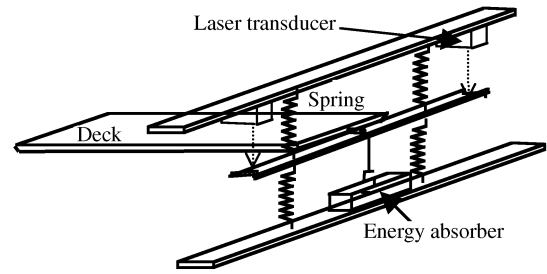


Fig. 3 Experimental setup

respectively 0.03 m and 0.15 m. (The blockage ratio is below 4%.) An additional energy absorber, filled with a viscous liquid, is set to produce appropriate damping in the vertical and torsional directions. Hot-film anemometry is used to measure the approaching flow speed. Moreover, four laser transducers are set on the rack mechanism to monitor the motion of the vibrating model deck. Other related physical quantities are illustrated in Table 1.

IV. RESULTS

1. Relative Error Resulting from the Selected Domain and Meshes in Flow Computations

To investigate the accuracy of the result of flow calculations by using the selected computational domain and meshes ($38D \times 16D$ with a grid size of 242×88), an additional flow calculation was performed in a larger computational domain and finer meshes ($70D \times 32D$ with a grid size of 424×216) for a trapezoidal deck with a zero attack angle ($\beta=0$) at a typical approaching flow speed ($U=7.4\text{ m/s}$). The comparisons in Table 2 show that the relative errors of the resulting mean and root-mean-square force coefficients in the vertical and torsional directions ($C_L = F_L/\rho U^2 B$ and $C_M = F_M/\rho U^2 B^2$; “-” and “” denote the mean and the root-mean-square values) are within 2%.

2. Verification of the Numerical Method

Figure 4 shows the comparisons of the root-mean-square values of the vertical and torsional deck deflections at various approaching wind speeds. It is noted that the figures are also presented in terms of the reduced velocities associated with the fundamental frequency in the cross-wind direction ($U_r = U/(f_v B)$). It can be seen that a good agreement between the results of measurements and numerical predictions is obtained.

In addition to those from the present section model experiments, available data from three other wind tunnel measurements are selected and compared with the results from the numerical predictions. Among the selected cases, Case 1 is associated with

Table 2 Comparison of the results of flow calculations

Domain and meshes	38D×16D 242×88 meshes	70D×32D 424×216 meshes	Relative error (%)
\overline{C}_L	-0.308	-0.307	0.33
C_L'	0.350	0.352	0.57
\overline{C}_M	0.098	0.099	1.01
C_M'	0.392	0.393	0.25

Table 3 Related properties of other experiments

	Mass (M) (kg/m)	Moment of inertia (I) (kg-m ² /m)	Fundamental frequency (Hz)		Damping ratio (%)	
			Vertical (f_V)	Torsional (f_T)	Vertical (ξ_V)	Torsional (ξ_T)
Case 1*	4.01 (Noda <i>et al.</i> , 2003)	0.0706	10.31	29.7	0.81	0.66
Case 2**	4.19 (Gu <i>et al.</i> , 2000)	0.0612	2.55	5.06	1.72	1.82
Case 3***	11.93 (Iwamoto and Fujino, 1995)	0.091	1.875	3.624	0.5	0.4

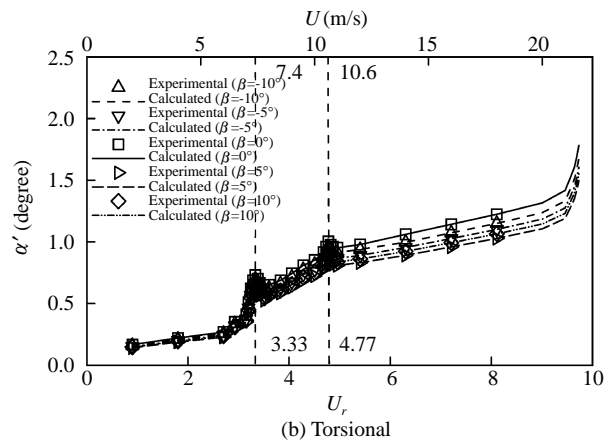
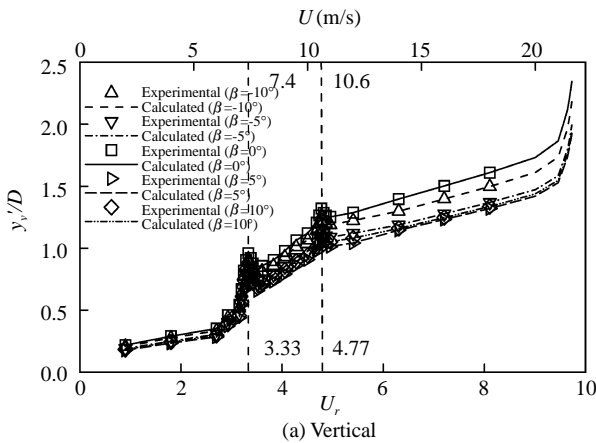
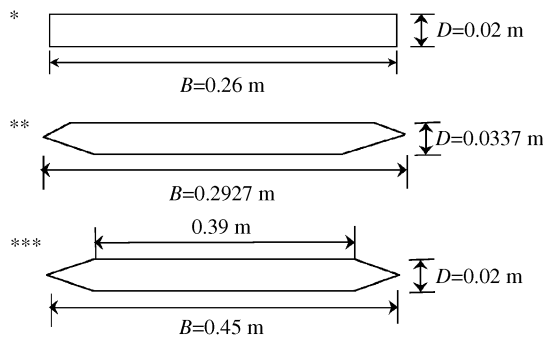


Fig. 4 Root-mean-square deflections at various wind speeds

a rectangular deck shape (Noda *et al.*, 2003); Cases 2 (Gu *et al.*, 2000) and 3 (Iwamoto and Fujino, 1995) are in relation to hexagonal cross-sections (see Table 3 for deck properties).

Compared to the experimental results from Noda *et al.* (2003), Fig. 5 shows the calculated variations

of normalized mean force coefficients with respect to the attack angles ($\overline{C}_L = \overline{F}_L / \rho U^2 B$ and $\overline{C}_M = \overline{F}_M / \rho U^2 B^2$; \overline{F}_L and \overline{F}_M are respectively the mean wind loads in the cross-wind and torsional directions). Fig. 6 illustrates the comparisons of the normalized mean and fluctuating pressure distributions along the upper

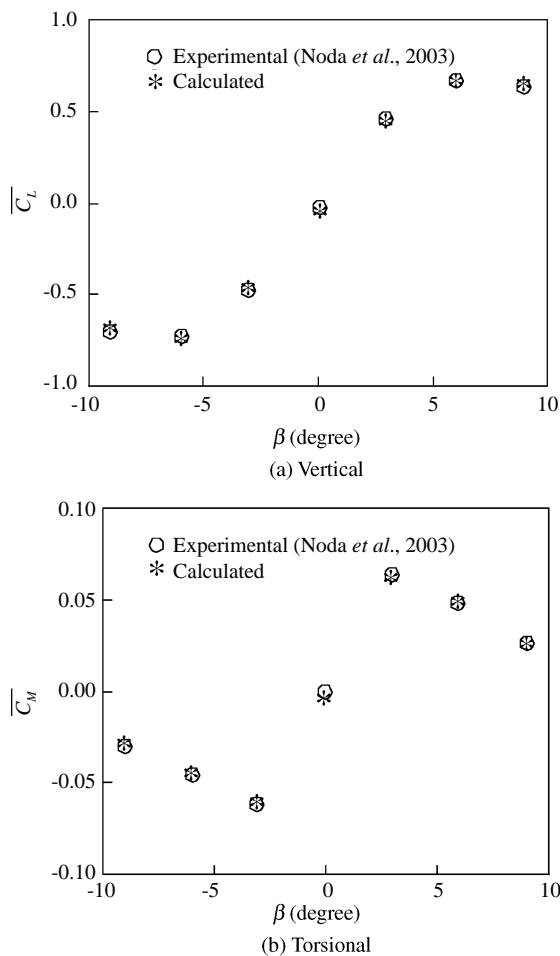


Fig. 5 Comparisons of mean force coefficients

surface of the rectangular deck ($\overline{C}_p = (p - p_o) / (0.5\rho U^2)$ and $C_p' = p' / (0.5\rho U^2)$; p_o is the approaching-flow pressure and p' is the root-mean-square value of local pressure). Additionally, Fig. 7 depicts the comparisons of flutter derivatives. All the results reveal that the deck motions are well predicted.

Considering the occurrence of flutter, on the other hand, Table 4 shows that the predicted critical speeds (U_{cr}) are in good agreement with those from the experiments (Gu *et al.*, 2000; Iwamoto and Fujino, 1995), indicating again that the proposed numerical method is capable of predicting the deck motions with good accuracy.

3. Deck Responses

For the present trapezoidal bridge deck, Fig. 4 shows that the root-mean-square deflections in both directions increase as the wind speed (or the reduced velocity) increases, except when two resonances occur (as U reaches 7.4 m/s and 10.6 m/s), leading to the occurrence of local peak values. To avoid damage of the deck model, unfortunately, the wind speed in

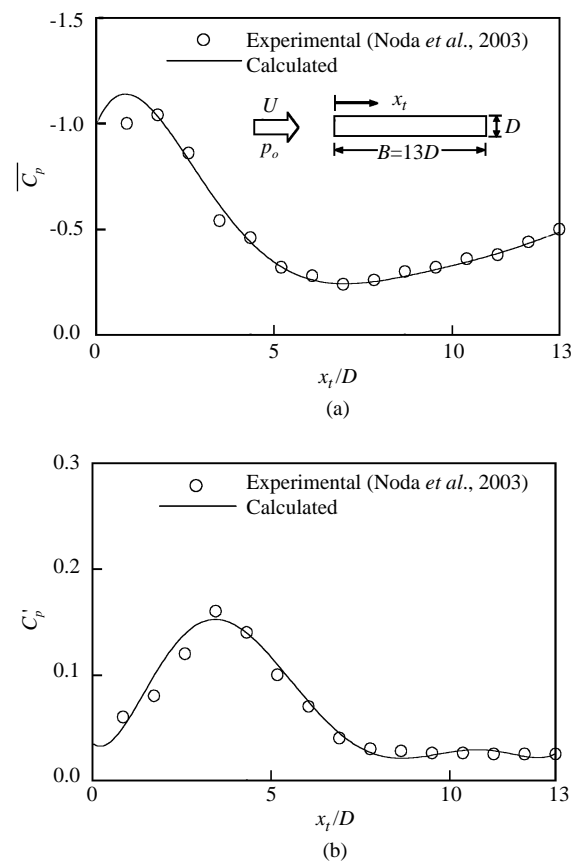


Fig. 6 Comparisons of mean and root-mean-square pressure coefficients

the experiments is limited to about 18 m/s. The numerical results, however, show that the root-mean-square deflections increase dramatically as the wind speed exceeds about 21.0 m/s. When U is about 21.6 m/s, numerical predictions show that the fluctuating responses in both the directions diverge, indicating the occurrence of flutter. Fig. 8 shows the variation of the resulting critical speeds (U_{cr}) at various attack angles. It appears that the effect of β is mild.

Evidence in Fig. 4 also shows that when $\beta=0^\circ$ the largest deflected responses are produced; the second largest deflections are found as the attack angle is -10° and the smallest responses occur at an attack angle of 5° .

4. Wind Loads

Based on the numerical results, normalized root-mean-square force coefficients in the cross-wind (lift) and torsional directions are shown in Fig. 9 for cases with and without the effect of interactions, in which calculations, in the latter cases, were performed based on a non-interactive procedure. Without considering the effect of interaction, first, the normalized root-mean-square force coefficients remain constant in

Table 4 Comparisons of the resulting critical flutter velocity

	Critical flutter velocity (U_{cr}) (m/s)	
	Experimental	Calculated
Case 2 (Gu et al., 2000)	19.5	19.65
Case 3 (Iwamoto and Fujino, 1995)	16.5	16.65

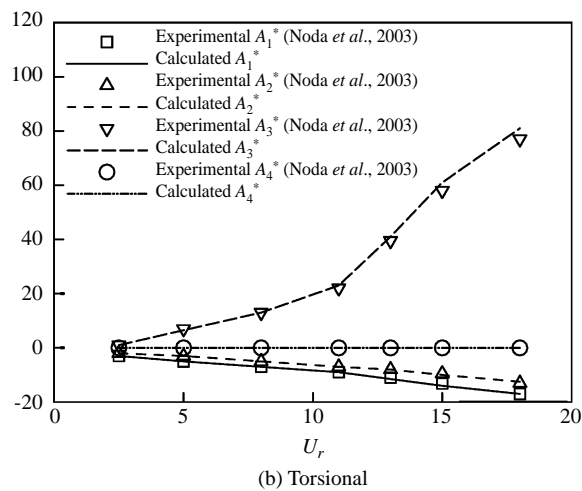
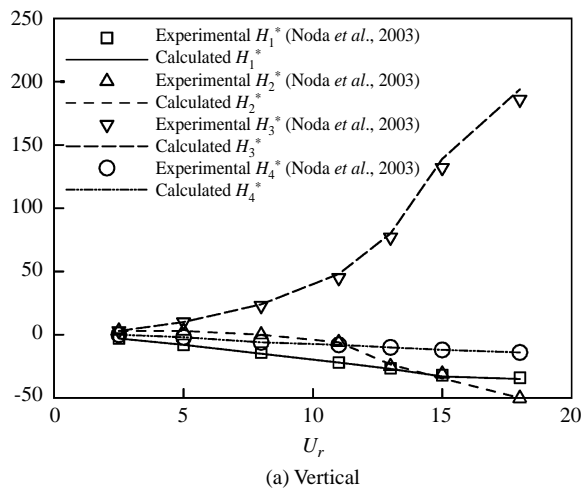


Fig. 7 Comparisons of flutter derivatives

both the cross-wind and torsional directions. However, discrepancies are found at various attack angles. Among all the cases, the one with a zero attack angle ($\beta=0^\circ$) results in the lowest values ($C_L'=0.126$ and $C_M'=0.134$), while the largest values ($C_L'=0.301$ and $C_M'=0.319$) are found when β is equal to 5° . In the interactive cases, on the other hand, the fluctuating force coefficients associated with both the cross-wind and torsional directions generally increase

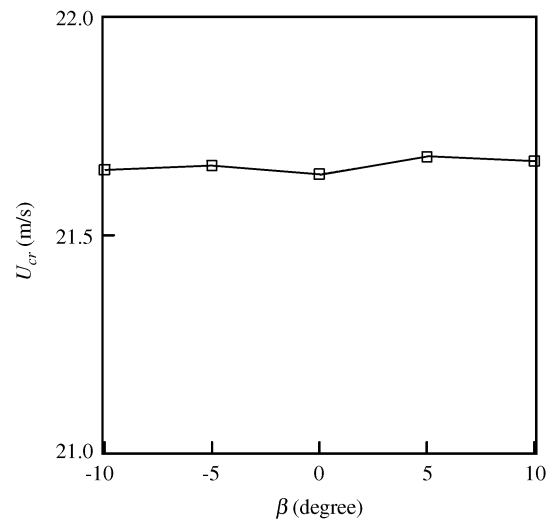


Fig. 8 Calculated critical flutter velocities at various attack angles

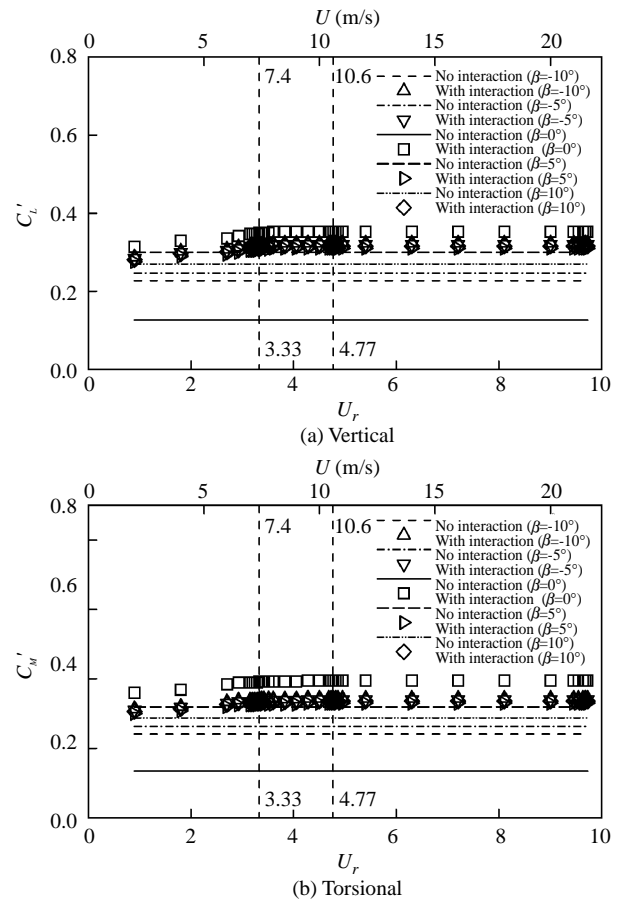


Fig. 9 Calculated root-mean-square aerodynamic force coefficients at various wind speeds

mildly at low wind speeds then tend to constant values as the wind speed increases. Moreover, the effect due to a change of the attack angle appears insignificant, except that the largest values occur in the case of a zero attack angle.

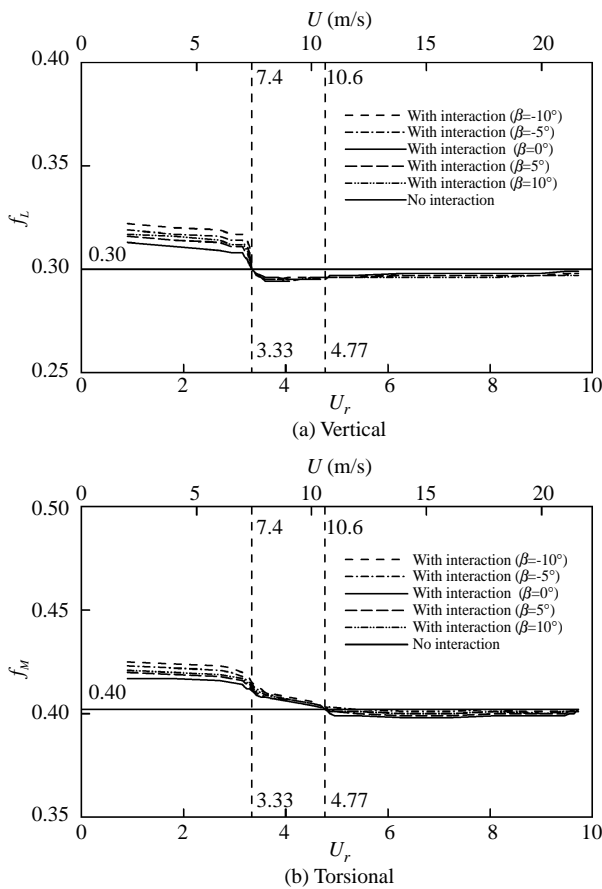


Fig. 10 Calculated normalized force frequencies at various wind speeds

To further investigate the effect of interaction on the wind loads, calculated normalized frequencies (f_L and f_M) associated respectively with the wind loads in the cross-wind and torsional directions are plotted in relation to the corresponding wind speeds (see Fig. 10). Generally, f_L and f_M decrease as U increases at low approaching speeds. When U reaches 7.4 m/s and 10.6 m/s, the normalized force frequencies match with the fundamental reduced frequencies (the reciprocals of 3.33 and 4.77) of the deck respectively in the vertical and torsional directions, indicating the occurrence of resonance in the corresponding direction. After exceeding the corresponding resonance wind speeds, f_L and f_M overshoot to smaller values compared to the non-interactive ones (0.3 and 0.4 respectively in the cross-wind and torsional directions) then gradually approach to the non-interactive values. Besides, the dependence on the attack angle appears mild within this high-speed range.

5. Aerodynamic Damping

Based on the numerical results, Fig. 11 shows the variations of the net damping ratios at various

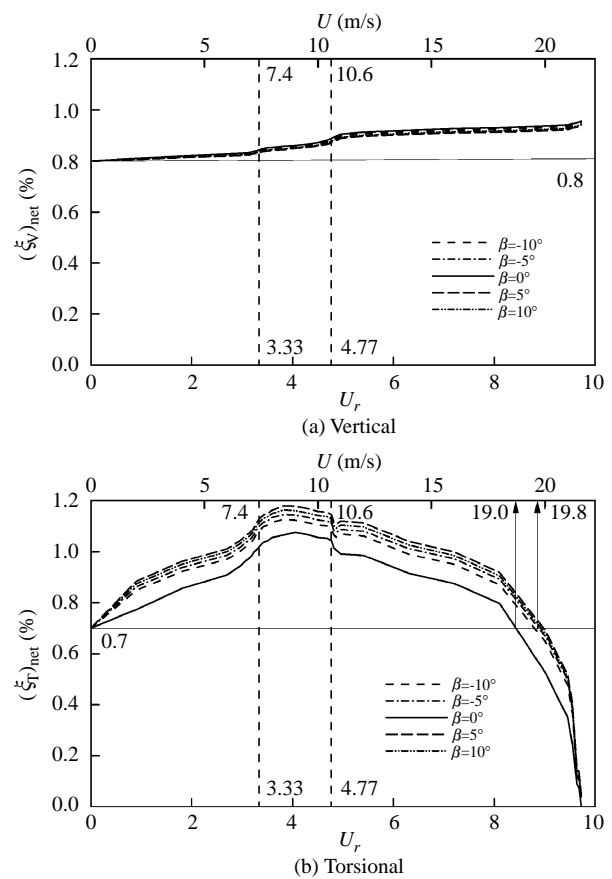


Fig. 11 Calculated net damping ratios at various wind speeds

approaching wind speeds. In the cross-wind direction (Fig. 11a), the variations of the net damping ratios start from the value of the material damping (0.8%) then increase with an increase of the wind speed. Also, the effect due to the change of β appears insignificant. In the torsional direction, in contrast, the variation pattern of the net damping ratios appears rather different. Peak values are detected in the range between the two resonance speeds. As the wind speed is about 19 m/s, the net damping ratios become less than the material damping (0.7%). Finally, they drop to zero values as U approaches about 21.6 m/s. Among all the cases, furthermore, the one with a zero attack angle results in the lowest net damping.

6. Flutter Derivatives

Figure 12 shows the flutter derivatives, typically, as β is equal to zero. It can be seen that those related to the aeroelastic force in the cross-wind direction (H_1^* to H_4^*) are all negative (Fig. 12a). In the torsional direction, on the other hand, all derivatives are positive except the one associated with the torsional speed (A_2^*), which is initially negative at

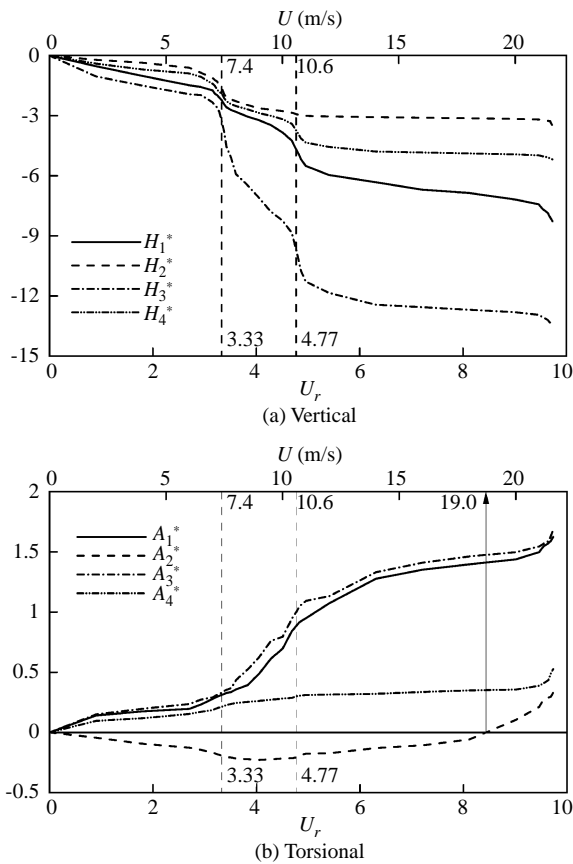


Fig. 12 Calculated flutter derivatives at various wind speeds ($\beta=0^\circ$)

lower wind speeds then becomes positive when U exceeds 19.0 m/s.

V. DISCUSSION

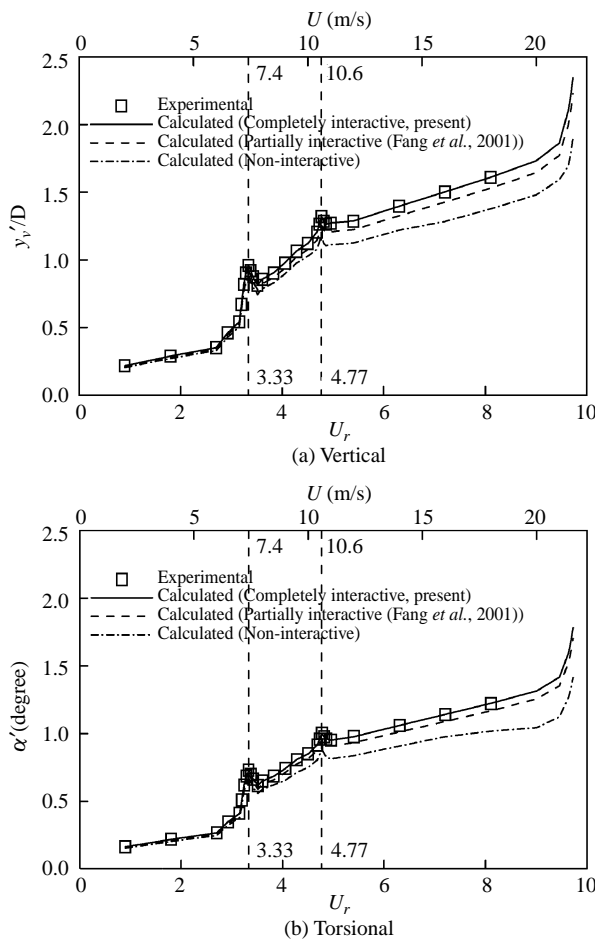
As the results from the measurements are treated as the prototype data for verifications, the application of the proposed numerical method has been proved to be quite successful in predicting the dynamic behaviors of the deck and the surrounding flow, which are actually interacting with each other. The variations of the root-mean-square deflections are well predicted (Fig. 4), even when resonances and flutter occur. Moreover, other important features associated with the deck motion (such as the characteristics of the wind forces, flutter derivatives and net damping ratios) are obtained. The good comparisons in Figs. 4 to 7 demonstrate the applicability of the proposed numerical method.

An important achievement in the proposed numerical method is the adoption of the coordinate transformation, which allows for execution of flow calculations on a fixed grid system. This is considered a major improvement in the weakly-compressible-flow method because it leads to not only significant

savings of computing time for grid generations in flow calculations but also avoidance of certain technical difficulties in the application of the dynamic turbulence model. A previous work carried out by Fang *et al.* (2001) used a partial interactive approach to simulate the response of a bridge deck with a rectangular cross-section. In their work, as the torsional responses were relatively insignificant (since the torsional stiffness was quite large), the coordinate transformation considered solely the part due to the cross-wind vibrations. Considering the interaction effect contributed by torsional motions of the deck, on the other hand, the boundary conditions at the deck surface were specified in such a way that the effect of vibrating angular velocities were physically reflected. To examine the difference of the predicted results between the previous (partially interactive procedure) and the present (completely interactive procedure) methods, additional numerical calculations were performed typically in the case of a zero attack angle. In terms of the root-mean-square cross-wind and torsional deflections, Fig. 13 shows that the predictions based on the present method with an interactive procedure are the closest to the experimental results. Meanwhile, Fig. 13 also reveals that the results from the non-interactive procedure lead to the largest errors since the effect of interaction is not included. As the interaction effect is partially reflected, the results are under-predicted by an order of 10% at a large wind speed.

Examinations on the tendency of the variations of root-mean-square deflections in Fig. 4 reveal that the fluctuating responses in both directions increase generally with an increase of the approaching speed. As U approaches 7.4 and 10.6 m/s, the peak responses are obtained obviously due to the occurrence of resonance (or the effect of vortex-induced vibration). At these two wind speeds, additional evidence in Fig. 10 shows that the force frequency in each direction matches with that of the corresponding fundamental frequency.

In the present case of study, the mechanism of the occurrence of flutter can be explored by examining the variations of the net damping ratios. Fig. 11a shows that the net damping in the translation mode (vertical or cross-wind direction) is always larger than the material damping. (The same evidence can also be detected in Fig. 12a, which shows all negative H_1^* values in the entire range of U .) By investigating the result in Fig. 11b, on the other hand, it can be seen that the net damping in the rotational mode (torsional direction) drops to zero at the critical speed. Accordingly, one can then conclude that although the fluctuating responses diverge in both directions (Fig. 4) at the critical flutter speeds, the instability of the deck is in reality initiated by torsional flutter. It is also noted that the net torsional damping becomes identical to that of the material damping as U is about

Fig. 13 Comparisons of root-mean-square deflections ($\beta=0^\circ$)

19 m/s, corresponding to the instant that A_2^* changes its sign (Fig. 12b). In addition, the reason why the largest fluctuating rotational response is found as $\beta=0^\circ$ can be explained based on the result in Fig. 11b, which shows the smallest net damping at the zero attack angle.

The fact that the most significant fluctuating responses are detected at a zero attack angle (Fig. 4) is quite interesting since its corresponding non-interactive fluctuating wind forces are minimum (Fig. 9). A similar concern is found in the case of the 5° attack angle, on the other hand, with an opposite outcome. Based on the numerical results, extensive examinations on the individual parts of the aeroelastic force in the vertical direction (associated respectively with H_1^* to H_4^*) are depicted in Fig. 14 for cases of the two attack angles (0° and 5°). In addition, the combined forces, resulting from the total aeroelastic forces minus the ones associated with H_1^* , are also presented. It can be seen that the combined forces, which are responsible for promoting the fluctuating responses of the deck, are mainly contributed by the part associated with H_2^* . With roughly the same net damping (see Fig. 11a), as the combined areoelastic

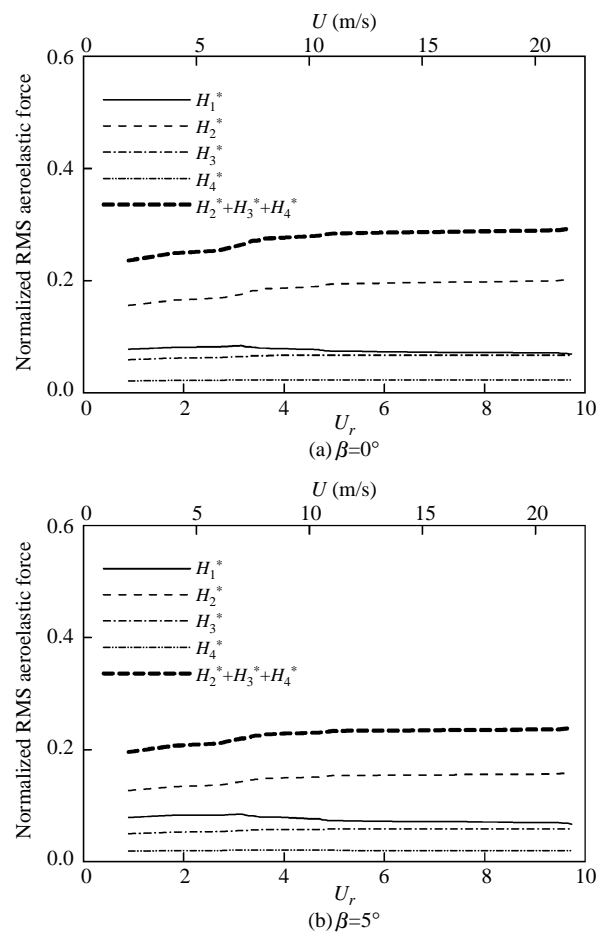


Fig. 14 Comparisons of aeroelastic forces in the vertical direction

force induced by the deck motion at a zero attack angle is greater than that of the case as $\beta=5^\circ$, the corresponding fluctuating responses of the former case therefore become larger.

VI. CONCLUSION

The proposed numerical model has been proved to be adequate in predicting the wind effects as well as the dynamic behavior of a suspension bridge with a trapezoidal cross-section. By introducing the technique of coordinate transformations in the governing equations of flow calculations, the computations are performed without the application of a dynamic grid system. This indeed improves the computation efficiency substantially. Finally, besides the predictions of the deck responses, the interaction mechanism of the vibrating bridge deck is discussed extensively based on the numerical results.

ACKNOWLEDGMENTS

The study was cordially funded by the National

Science Council in Taiwan (grant Nos. NSC 90-2211-E-005-024 and NSC 92-2211-E-005-028).

NOMENCLATURE

B	width of deck upper surface
$\overline{C_L}, \overline{C_M}$	mean lift and moment coefficients
C_L', C_M'	fluctuating lift and moment coefficients
$\overline{C_p}, C_p'$	mean and root-mean-square pressure coefficients
D	deck thickness
F_L, F_M	wind loads in the cross-wind and torsional directions
$(F_L)_I, (F_M)_I$	aeroelastic forces in the cross-wind and torsional directions
f_L, f_M	normalized force frequencies
f_V, f_T	fundamental frequencies of deck in the cross-wind and torsional directions
H_j^*, A_j^*	flutter derivatives
I	moment of inertia of deck
K	$2\pi f_V B/U$
k	bulk modulus of elasticity
M	mass of deck
p	pressure
U	approaching-flow speed
U_r	reduced velocity
U_{cr}	critical flutter velocity
u, v	velocity components
X, Y	moving spatial coordinates
x, y	original spatial coordinates
y_V	deck deflection in the cross-wind direction
\dot{y}_V	speed of deck vibration in the cross-wind direction
\ddot{y}_V	acceleration of deck vibration in the cross-wind direction
y_V'	root-mean-square deck deflection in the cross-wind direction
α	deck deflection in the torsional direction
$\dot{\alpha}$	speed of deck vibration in the torsional direction
$\ddot{\alpha}$	acceleration of deck vibration in the torsional direction
α'	root-mean-square deck deflection in the torsional direction
β	attack angle
θ	inclined angle of deck side surfaces
ρ	fluid density
ω_V, ω_T	circular frequencies
ξ_V, ξ_T	material damping ratios
ν, ν_t	absolute and turbulent viscosities

REFERENCES

- Courant, R., Friedrichs, K. O., and Lewy, H., 1967, "On the Partial Difference Equations of Mathematical Physics," *IBM Journal*, Vol. 11, No. 2, pp. 215-234.
- Fang, F. M., Li, Y. C., Chen, C. C., Chen, J. H., and Ueng, J. M., 2001, "Dynamic Responses of a Suspension Bridge with a Rectangular Cross-section," *Proceedings of the 5th Asia-Pacific Symposium on Wind Engineering*, Kyoto, Japan, pp. 397-400.
- Germano, M., Piomelli, U., Moin, P., and Cabot, W. H., 1991, "A Dynamic Subgrid-Scale Eddy Viscosity Model," *Physics of Fluids*, Vol. 3, pp. 1760-1765.
- Gu, M., Zhang, R., and Xiang, H., 2000, "Identification of Flutter Derivatives of Bridge Decks," *Journal of Wind Engineering and Industrial Aerodynamics*, Vol. 84, No. 7, pp. 151-162.
- Iwamoto, M., and Fujino, Y., 1995, "Identification of Flutter Derivatives of Bridge Deck from Free Vibration Data," *Journal of Wind Engineering and Industrial Aerodynamics*, Vol. 54/55, pp. 55-63.
- Kuroda, S., 1997, "Numerical Simulation of Flow around a Box Girder of a Long Span Suspension Bridge," *Journal of Wind Engineering and Industrial Aerodynamics*, Vol. 67/68, pp. 239-252.
- Lee, S., Lee, J. S., and Kim, J. D., 1997, "Prediction of Vortex-induced Wind Loading on Long-span Bridge," *Journal of Wind Engineering and Industrial Aerodynamics*, Vol. 67/68, pp. 267-278.
- Noda, M., Utsunomiya, H., Nagao, F., Kanda, M., and Shiraishi, N., 2003, "Effects of Oscillation Amplitude on Aerodynamic Derivatives," *Journal of Wind Engineering and Industrial Aerodynamics*, Vol. 91, pp. 101-111.
- Sarkar, P. P., Jones, N. P., and Scanlan, R. H., 1992, "System Identification for Estimation of Flutter Derivatives," *Journal of Wind Engineering and Industrial Aerodynamics*, Vol. 41-44, pp. 1243-1254.
- Scanlan, R. H., and Tomko, J. J., 1971, "Airfoil and Bridge Deck Flutter Derivatives," *Journal of Engineering Mechanics Division*, Vol. 97, No. EM6, pp. 1717-1737.
- Song, C. C. S., and Yuan, M., 1998, "A Weakly Compressible Flow Model and Rapid Convergence Methods," *Journal of Fluids Engineering*, Vol. 110, No. 4, pp. 441-455.

Manuscript Received: Dec. 08, 2003

Revision Received: Apr. 22, 2004

and Accepted: Jun. 10, 2004